

NASA/CR-2001-211223
ICASE Report No. 2001-27



Progressive Failure Studies of Composite Panels with and without Cutouts

*Navin Jaunky
ICASE, Hampton, Virginia*

*Damodar R. Ambur, Carlos G. Dávila, and Mark Hilburger
NASA Langley Research Center, Hampton, Virginia*

*ICASE
NASA Langley Research Center
Hampton, Virginia*

Operated by Universities Space Research Association



National Aeronautics and
Space Administration

Langley Research Center
Hampton, Virginia 23681-2199

Prepared for Langley Research Center
under Contract NAS1-97046

September 2001

Report Documentation Page

Report Date 00SEP2001	Report Type N/A	Dates Covered (from... to) -
Title and Subtitle Progressive Failure Studies of Composite Panels with and without Cutouts	Contract Number	
	Grant Number	
	Program Element Number	
Author(s) Navin Jaunky	Project Number	
	Task Number	
	Work Unit Number	
Performing Organization Name(s) and Address(es) National Aeronautics and Space Administration Langley Research Center Hampton, Virginia 23681-2199	Performing Organization Report Number	
Sponsoring/Monitoring Agency Name(s) and Address(es)	Sponsor/Monitor's Acronym(s)	
	Sponsor/Monitor's Report Number(s)	
Distribution/Availability Statement Approved for public release, distribution unlimited		
Supplementary Notes ICASE Report No. 2001-27		
Abstract Abstract. Progressive failure analyses results are presented for composite panels with and without a cutout and subjected to in-plane shear loading and compression loading well into their postbuckling regime. Ply damage modes such as matrix cracking, ber-matrix shear, and ber failure are modeled by degrading the material properties. Results from nite element analyses are compared with experimental data. Good agreement between experimental data and numerical results are observed for most structural con gurations when initial geometric imperfections are appropriately modeled.		
Subject Terms		
Report Classification unclassified	Classification of this page unclassified	
Classification of Abstract unclassified	Limitation of Abstract SAR	
Number of Pages 23		

PROGRESSIVE FAILURE STUDIES OF COMPOSITE PANELS WITH AND WITHOUT CUTOUTS

NAVIN JAUNKY*, DAMODAR R. AMBUR†, CARLOS G. DÁVILA‡, AND MARK HILBURGER§

Abstract. Progressive failure analyses results are presented for composite panels with and without a cutout and subjected to in-plane shear loading and compression loading well into their postbuckling regime. Ply damage modes such as matrix cracking, fiber-matrix shear, and fiber failure are modeled by degrading the material properties. Results from finite element analyses are compared with experimental data. Good agreement between experimental data and numerical results are observed for most structural configurations when initial geometric imperfections are appropriately modeled.

Key words. composite structures, progressive failure, ply damage mode, buckling, postbuckling

Subject classification. Structural Mechanics

1. Introduction. The use of composite materials for aircraft primary structures can result in significant benefits on aircraft structural cost and performance. Such applications of composite materials are expected to result in a 30-40 percent weight savings and a 10-30 percent cost reduction compared to conventional metallic structures. However, unlike conventional metallic materials, composite structures fail under different failure modes such as matrix cracking, fiber-matrix shear failure, fiber failure, and delamination. The initiation of damage in a composite laminate occurs when a single ply or part of the ply in the laminate fails in any of these failure modes over a certain region of the structure. The initiation of damage does not mean that the structure cannot carry any additional load. The residual load bearing capability of the composite structure from the onset of material failure or initiation of damage to final failure can be quite significant. It is beyond the final failure point that the structure cannot carry any further load. This may be due to the fact that some failure modes may be benign not to degrade the performance of the overall structure significantly. Accurate determination of failure modes and their progression while the structure is loaded helps either to devise structural features for damage containment or to define fail-safe criteria. It is, therefore important to understand the damage progression in composite structures subjected to different single and multi-component loading conditions.

Considerable work has been performed on this subject. In 1987, Talreja ([1]), Allen et al. ([2]), and Chang and Chang ([3]), independently proposed progressive failure models that describe the accumulation of damage in a composite laminate by a field of internal state variables. Also in the same year, progressive failure analyses were presented in References [4] and [5]. A summary of the past work in progressive failure taking into account the type of structure analyzed and the loading condition is presented in Table 1.

Table 1 indicates that nonlinear geometric effects were initially not considered. However material non-linearity was considered in References [3, 6] and [9]. Englestad et al. ([8]) were among the first researchers

*Senior Staff Scientist. ICASE, NASA Langley Research Center, Hampton, VA 23681-2199. This research was supported by the National Aeronautics and Space Administration under NASA Contract No. NAS1-97046 while the first author was in residence at ICASE, NASA Langley Research Center, Hampton, VA 23681-2199.

†Head, Mechanics and Durability Branch. NASA Langley Research Center, Hampton, VA 23681-2199

‡Aerospace Engineer, Analytical & Computational Methods Branch. NASA Langley Research Center, Hampton, VA 23681-2199

§Aerospace Engineer, Mechanics and Durability Branch. NASA Langley Research Center, Hampton, VA 23681-2199

to consider nonlinear geometric effects and subsequently consider a postbuckling problem with progressive failure. Experimental correlation with progressive failure analyses were mostly attempted at the coupon level. Comparison of progressive failure analyses with experimental data for structures of realistic size was presented in Reference [8] and later in References [11] and [12]. Recently in References [16] and [17] experimental correlation with progressive failure analyses for stiffened panels were presented. Baranski and Biggers ([18]) used progressive failure analyses to show that the failure and buckling load of composite panels subjected to compression can be enhanced by appropriate stiffness tailoring. Progressive failure analyses of panels presented in References [13, 15, 14] and [19] indicate that progressive failure analyses can be used to provide better assessment of a structure at an advanced design stage. The survey also indicates that work on progressive failure analyses of curved panels is lacking.

The objective of the present paper is to develop and validate an efficient methodology that can predict the ultimate strength of composite panels by taking into account ply damage modes and geometrical non-linear response. Results from progressive failure analyses of composite panels with and without cutouts and subjected to shear and compressive loads are compared with existing experimental results. Progressive failure analysis results are compared with experimental results for flat panels with and without a cutout and subjected to in-plane shear loading. Progressive failure results are also presented for curved panels with and without cutouts and subjected to axial compression.

2. Failure Analysis. Failure modes in laminated composite panels are strongly dependent on ply orientation, loading direction and panel geometry. There are four basic modes of failure that occur in a laminated composite structure. These failure modes are; matrix cracking, fiber-matrix shear failure, fiber failure, and delamination. Delamination failure, however, is not included in the present studies. In order to simulate damage growth accurately, the failure analysis must be able to predict the failure mode in each ply and apply the corresponding reduction in material stiffnesses. The failure criteria included in the present analyses are those proposed by Hashin [21] and are summarized below.

- Matrix failure in tension and compression occurs due to a combination of transverse, σ_{22} , and shear stress, τ_{12} , τ_{13} and τ_{23} . The failure index can be defined in terms of these stresses and the strength parameters Y and shear allowables S_c . Failure occurs when the index, e_m , exceeds unity. Assuming linear elastic response, the failure index has the form:

$$(2.1) \quad e_m^2 = \frac{\sigma_{22}}{Y_c} \left[\left(\frac{Y_c}{2S_{c23}} \right)^2 - 1 \right] + \left(\frac{\sigma_{22}}{2S_{c23}} \right)^2 + \left(\frac{\tau_{12}}{S_{c12}} \right)^2 + \left(\frac{\tau_{13}}{S_{c13}} \right)^2 + \left(\frac{\tau_{23}}{S_{c23}} \right)^2 \text{ for } \sigma_{22} < 0$$

and

$$(2.2) \quad e_m^2 = \left(\frac{\sigma_{22}}{Y_t} \right)^2 + \left(\frac{\tau_{12}}{S_{c12}} \right)^2 + \left(\frac{\tau_{13}}{S_{c13}} \right)^2 + \left(\frac{\tau_{23}}{S_{c23}} \right)^2 \text{ for } \sigma_{22} > 0$$

where Y_t is the strength perpendicular to the fiber direction in tension, Y_c is the strength perpendicular to the fiber direction in compression, and S_{c12} , S_{c13} , and S_{c23} are the in-plane shear and transverse shear strengths, respectively.

- Fiber-matrix shear failure occurs due to a combination of axial stress (σ_{11}) and the shear stresses. The failure criterion has the form:

$$(2.3) \quad e_s^2 = \left(\frac{\sigma_{11}}{X_c} \right)^2 + \left(\frac{\tau_{12}}{S_{c12}} \right)^2 + \left(\frac{\tau_{13}}{S_{c13}} \right)^2 \text{ for } \sigma_{11} < 0$$

and

$$(2.4) \quad e_s^2 = \left(\frac{\tau_{12}}{S_{c12}} \right)^2 + \left(\frac{\tau_{13}}{S_{c13}} \right)^2 \quad \text{for } \sigma_{11} > 0$$

where X_t is the strength along the fiber direction in tension, and X_c is the strength along the fiber direction in compression.

- Fiber failure occurs due to tension or compression independent of the other stress components. In compression, the fiber fails by micro-buckling. The failure criterion has the form:

$$(2.5) \quad e_f = \frac{-\sigma_{11}}{X_c} \quad \text{for } \sigma_{11} < 0$$

and

$$(2.6) \quad e_f = \frac{\sigma_{11}}{X_t} \quad \text{for } \sigma_{11} > 0$$

To simulate the above failure modes, the elastic properties are made to be linearly dependent on three field variables, $FV1$, $FV2$, and $FV3$. The first field variable represents the matrix failure, the second the fiber-matrix shearing failure, and the third the fiber buckling failure. The values of the field variables are set equal to zero in the undamaged state. After a failure index has exceeded 1.0, the associated user-defined field variable is set equal to 1.0. The associated field variable then continues to have the value of 1.0, even though the stresses may reduce to values lower than the failure stresses of the material. This procedure ensures that the damaged material does not heal. The mechanical properties in the damaged area are reduced appropriately, according to the property degradation model defined in Table 2. For example, when the matrix failure criterion takes the value of 1.0, then by the interpolation rule defined in Table 2, the transverse shear modulus (E_y) and the Poisson ratio (ν_{12}) are set equal to zero. The field variables can be made to transit from 0 (undamaged) to 1 (fully damaged) instantaneously. Chang and Lessard's degradation model [6] is used in the present study.

The finite element implementation of this progressive failure analysis was developed for the ABAQUS structural analysis program using the USDFLD user-written subroutine [22, 23]. ABAQUS calls this USDFLD subroutine at all material points of elements that have material properties defined in terms of the field variables. The subroutine provides access points to a number of variables such as stresses, strains, material orientation, current load step, and material name, all of which can be used to compute the field variables. Stresses and strains are computed at each incremental load step and evaluated by the failure criteria to determine the occurrence of failure and the mode of failure.

3. Numerical Examples. To assess the predictive capability of the present failure analysis method, several panels have been analyzed and these results were compared with experimental results. Results are presented for unstiffened panels with and without cutouts and a stiffened panel. The unstiffened panel cases are flat panels loaded in shear and curved panels loaded in compression. Results are also presented for a bead-stiffened panel subjected to in-plane shear loading.

3.1. Flat Panel Loaded in In-plane Shear. The flat panels were loaded using a picture frame fixture to subject it to a pure in-plane shear loading. The test sections of the panel is 12.0-in. by 12.0-in. in size and the members of the picture frame were 2.75-in. wide and 6.75-in thick. The fixture is made of steel. Figure 1 shows a schematic diagram of the picture frame test fixture. In the finite element model, nodes on each member were constrained for the out-of-plane displacement. Pin joint consists of two co-incident nodes tied

in a multi-point constraint at the four corners of the panel. The displacements of the dependent node are made the same as that of the independent node, but the rotations of the co-incident nodes are not included in the multi-point constraints. The independent node diagonally opposite to the loading pin is constrained in the axial and transverse displacements. At the loading pin, applied displacement equal in magnitude in the axial and transverse directions at the independent node simulate the loading condition. The test section is modeled using ABAQUS four node, reduced integration, shear deformable S4R elements [23]. The members of the picture frame are modeled using ABAQUS four node shear deformable S4 elements [23].

The flat unstiffened panel has a laminate stacking sequence of $[\pm 45/0/90]_{2s}$, with a ply thickness of 0.0056-in. and is made of graphite epoxy. The mechanical properties for the material are $E_{11}=18.5$ Msi, $E_{22}=1.64$ Msi, $G_{12}=G_{13}=0.87$ Msi, $G_{23}=0.55$ Msi, and $\nu_{12}=0.3$. The strength allowables are $X_t=232.75$ ksi, $X_c=210.0$ ksi, $Y_t=14.7$ ksi, $Y_c=28.7$ ksi, $S_{c12}=S_{c13}=29.75$ Ksi, and $S_{c23}=4.8$ ksi. Experimental results for this test panel are reported in Reference [24].

A finite element model of that flat panel is shown in Figure 2. This model consists of 3425 nodes and 3300 elements. An imperfection based on static analysis results for a pressure load is added to the model to simulate an imperfect shape similar to that of a bubble (one half wave in each direction of the panel). Progressive failure analysis (PFA) is carried out for this case with a maximum imperfection magnitude equal to 5% of the laminate thickness. Three integration points through each ply thickness are used in the analysis for computation of section properties. A post-buckling analysis of the panel with the same level of imperfection is also performed.

The results for the flat panel loaded in shear are shown in Figure 3, where the load is plotted versus the strain normal to the fiber direction (ϵ_{22}) in the top and bottom plies (45° ply) at the center of the test specimen. The dashed lines marked FV1, FV2 and FV3 indicate the load levels at which damage described by field variable *FV1* through *FV3* are initiated well into the post buckling regime. These failures are due to severe bending. The thick solid line represents the experimental results and the thin solid line represents the postbuckling analysis results. The solid and open triangles are analytical results for the panel response with progressive failure. The analysis results are in good agreement with the experimental results until the initiation of all failure modes, well into the postbuckling regime. The final failure load obtained from the experiment is 54.81 kips, which is 6 % more than the final failure load of approximately 51.5 kips obtained from progressive failure analysis.

Damage initiation starts as matrix cracking (*FV1*) at a load level of 38 kips. Fiber-matrix shear (*FV2*), and fiber (*FV3*) failure are initiated at the same load level of 45 kips. This indicates that the structure can carry an additional load of 17 kips (about 30% of the final experimental load) after matrix cracking has been initiated. Even after the initiation of fiber-matrix shear and fiber failure, the panel continues to carry an additional load of approximately 9.4 kips (17% of the final experimental load). The post-buckling analysis results diverge from the progressive failure results at a load level that is slightly higher than the load at which initiation of fiber-matrix shear and fiber failure occurs. At that load level the analysis predicts a significant amount of damage that could have led to a considerable loss of panel stiffness.

All the failure modes initiated near the steel supporting fixture along the diagonal in the panel loading direction and propagate in the region close to this diagonal. Figure 4 shows an out-of-plane deflection fringe plot for the panel well after buckling which is similar to the mode shape observed in the experiment. Fringe plots of damage after the final failure load are shown in Figure 5(a) through 5(d) for matrix cracking in the top 45 degree ply, matrix cracking in the bottom -45 degree ply, fiber-shear matrix in the bottom -45 degree ply, and fiber failure in the bottom -45 degree ply, respectively. The dark contours denote damaged regions

of the panel. The location of damage for matrix cracking in the top 45 degree ply is within the central half wave of the out-of-plane deflection, whereas the location of matrix cracking in the bottom -45 degree ply is within the off-diagonal half waves and extends over a much larger extent. These locations of matrix cracking are region of maximum compressive strain normal to the fiber direction in the top 45 degree ply and bottom -45 degree ply. The fiber matrix shear and fiber failure damage in the bottom -45 degree ply is within the central half wave which is the location for maximum compressive strain along the fiber direction for that ply.

3.2. Curved Panel Loaded in Axial Compression. The curved panel has a laminate stacking sequence of $[\pm 45/0/90]_{3s}$, with a measured ply thickness of 0.00529-in. The mechanical properties of the material used for the panel are $E_{11}=17.5$ Msi, $E_{22}=1.51$ Msi, $G_{12}=G_{13}=0.78$ Msi, $G_{23}=0.55$ Msi, and $\nu_{12}=0.29$. The strength allowables are $X_t=206.0$ ksi, $X_c=206.0$ ksi, $Y_t=8.9$ ksi, $Y_c=17.8$ ksi, $S_{c12}=S_{c13}=18.3$ Ksi, and $S_{c23}=4.8$ ksi. Experimental results for this test are reported in Reference [25].

The panel geometry, boundary conditions and loading are shown in Figure 6. The panel finite element model consists of 6561 nodes and 6400 shear deformable S4R elements ([23]). Measured geometric imperfection from a typical test specimen was included in the model. Three integration points through each ply thickness are used in the analysis for computation of section properties. Progressive failure analyses are performed using both geometrically perfect and imperfect panel models.

The results for the curved panel loaded in compression are shown in Figure 7, where the load is plotted against the end-shortening displacement. The open symbols representing FV1, FV2, and FV3 indicate the load levels at which damage described by field variable $FV1$ through $FV3$ are initiated. The analysis results with geometric imperfection and the experimental results are in good agreement. The final failure load from the experiment is 51.25 kips, which is about 8% less than the final failure load obtained from progressive failure analysis that included geometric imperfection of 55.3 kips. Analysis results suggest that all damage modes initiate after the panel buckling which corresponds to its maximum load bearing capability. Matrix cracking ($FV1$) initiated at a load level of 47.9 kips just after buckling. Fiber-matrix shear ($FV2$) and fiber failure ($FV3$) initiated at a load level of 40.2 kips. Progressive failure analyses indicates that the perfect panel buckles at 64.4 kips, matrix cracking is initiated at this load, and fiber-shear matrix and fiber failure are initiated at 55.02 kips.

Figure 8(a) through 8(d) show contour plots of out-of-plane displacement from moire interferometry, fringe plots of matrix cracking ($FV1$) in the bottom ply, fiber-matrix shear ($FV2$) in the bottom ply, and fiber failure ($FV3$) in the bottom ply after final failure respectively. The moire contour plot is consistent with the deformed shape obtained from the progressive failure analysis where the half wavelength at the lower region of the panel has a larger displacement gradient. Analysis results indicates that damage initiated within the lower region of the deformed panel and propagated to the area shown in Figure 8(b) through 8(d). Damage also accumulated in part of the region supported by the knife edges of the fixture. These results are consistent with observations from the experiments which did not indicate delamination failure.

3.3. Flat Panel with a Cutout and Loaded in Shear. The flat unstiffened panel has a 1.0-inch diameter circular cutout and a laminate stacking sequence of $[\pm 45/0_2]_{3s}$, with a ply thickness of 0.0055-in. The test section is 12-in. square. The mechanical properties for the panel are $E_{11}=18.5$ Msi, $E_{22}=1.67$ Msi, $G_{12}=G_{13}=0.87$ Msi, $G_{23}=0.258$ Msi. The allowables are $X_t=200.0$ ksi, $X_c=180.0$ ksi, $Y_t=12.6$ ksi, $Y_c=24.6$ ksi, $S_{c12}=S_{c13}=25.5$ Ksi, and $S_{c23}=4.8$ ksi. The panel is loaded in a picture frame similar to the one described earlier. Experimental results for this test are reported in Reference [26].

The finite element model has 3117 nodes and 3029 shear deformable S4R elements ([23]) and is shown

in Figure 9. Geometric imperfection based on static analysis results for a pressure loaded panel was used to simulate an imperfect shape similar to one half wave in the axial and transverse directions of the panel. Since no measured geometric imperfection data was available, progressive failure analyses were carried out for this case with a maximum imperfection of magnitude equal to 5% and 1% of the laminate thickness. Three integration points through each ply thickness are used in the analysis for computation of section properties.

The load versus strain normal to the fiber direction (ϵ_{22}) on the top and bottom plies (45° ply) at a location 0.5-in. below the edge of the hole along the diagonal that is in the panel loading direction are shown in Figure 10. The largest analytical buckling load was for the case where the imperfection magnitude was 1% of the laminate thickness. The experimental buckling load is approximately 25.1 kips, whereas numerical buckling load is approximately 23.2 kips and 19.5 kips for the case of imperfections equal to 1% and 5% of laminate thickness, respectively. A more accurate prediction of buckling load can be obtained by using measured geometric imperfection which was not available for this case. Damage modes *FV1*, *FV2* and *FV3* initiated very near the edge of the hole at a load level of 28.17 kips which is above the buckling load as indicated by the dashed curve Figure 10. The experimental failure load is 42.6 kips whereas the predicted failure load is 47.3 kips (data not shown in Figure 10) or 11% above the experimental final failure load. Based on the prediction of initial failure, it seems that the panel can carry an additional load of 14.4 kips (33% of the experimental final failure load) before final failure. At approximately 36 kips the computed strain data begins to diverge from the experimental strain data. This divergence may be due to not accounting for the delamination failure that occurred in the test. A fringe plot of out-of-plane deflection and damage plot in the region around the hole for the bottom 45° ply are shown in Figure 11(a) through 11(d) at a load level just after final failure. These damage locations are consistent with experimental observations and occurs in a region of high displacement gradient as shown in Figure 11(a).

3.4. Curved Panel with a Cutout and Loaded in Compression. The curved panels investigated with cutouts have the same laminate stacking sequence and material properties as the curved panel without cutout described above. The dimensions and boundary conditions for the panel are described in Figure 6. These panels have a circular cutout that are centrally located. Three panels with different cutout sizes are considered such that the ratio of cutout diameter to the panel width, d/W , is 0.2, 0.4 and 0.6. Experimental results for this test are reported in Reference [25].

The finite element model consists of 4112 nodes and 3940 elements for panel with $d/W=0.2$, 3992 nodes and 3804 elements for the panel with $d/W=0.4$ and 3720 node and 3508 elements for panel with $d/W=0.6$. Shear deformable S4R elements ([23]) are used each model. Measured ply thicknesses are 0.00529-in. for panel with $d/W=0.2$ and 0.00542-in. for panel with $d/W=0.4$ and $d/W=0.6$. Measured geometric imperfection was included to the model. Three integration points through each ply thickness are used in the analysis for the computation of the section properties. Progressive failure analyses are performed for geometrically imperfect and perfect panels. For panels with $d/W=0.4$ and 0.6, postbuckling analyses was also performed for the geometrically imperfect panels.

3.4.1. Curved panel with a cutout of size $d/W=0.2$. The results for the curved panel with a cutout ratio (d/W) of 0.2 are presented in Figure 12, where the load is plotted versus the end-shortening displacement. The open symbols representing *FV1*, *FV2* and *FV3* indicate the load level at which damage described by field variable initiated. Damage initiated before panel buckling occurred. The analyses and experimental results are in good agreement for most of the loading range. The final failure load obtained from the experiment is 39.3 kips which is also the load where the panel failed catastrophically. The final

failure load obtained from progressive failure analysis is approximately 39.6 kips for the perfect panel and 36.2 kips for the imperfect panel which is approximately 8% less than the experimental failure load. The analysis results indicate that the imperfect panel failure at an end-shortening of 0.05025-in. which is in good agreement with the experimental results. Damage initiates as matrix cracking (*FV1*), fiber-matrix shear (*FV2*) and fiber (*FV3*) failure at a load level of 32.4 kips for the perfect panel whereas damage initiation occurs as fiber-matrix shear (*FV2*) and fiber (*FV3*) failure at a load level of 29.8 kips for the imperfect panel.

All the failure modes initiated near the edge of the cutout. Figure 15 shows a fringe plots of damage in the bottom ply after the final failure load for the geometrically imperfect panel. These damage location are consistent with regions of displacements gradient indicated by the moire fringe contours and is also consistent with experimental failure observations. Experimental observation also indicated significant delamination around the cutout. Although the initial geometric imperfection is accurately represented here, the delamination damage may be responsible for the discrepancy between the analytical and experimental failure loads with the panel exhibiting a catastrophic failure with no residual strength.

3.4.2. Curved panel with a cutout of size $d/W=0.4$. The results for the curved panel with a cutout ratio (d/W) of 0.4 are presented in Figure 13, where the load is plotted versus the end-shortening displacement. The open symbols representing *FV1*, *FV2* and *FV3* indicate the load level at which damage described by field variable *FV1* through *FV3* initiated. Damage initiated before panel buckling occurred. The analyses and experimental results are in good agreement for most part of the loading range. The final failure load obtained from the experiment is 27.2 kips. The final failure load obtained from progressive failure analysis is 27.6 kips for the geometrically perfect panel and 26.0 kips for the geometrically imperfect panel which is approximately 4% less than the experimental failure load. However both imperfect panel and perfect panel failed at approximately the same end-shortening levels which is larger than the experimental end-shortening at failure. Damage initiation starts as fiber-matrix shear (*FV2*) and fiber (*FV3*) failure at a load level of 21.7 kips for the perfect panel whereas damage initiation starts as fiber-matrix shear (*FV2*) and fiber (*FV3*) failure at a load level of 21.28 kips for the imperfect panel. A postbuckling analysis for the geometrically imperfect panel predicts stiffening and softening behaviors in the load-deflection curve which is due to a change in the deformed mode shape.

All the failure modes initiate near the edge of the cutout. Figure 15 shows a fringe plots damage in the bottom ply after the final failure load for the geometrically imperfect panel. These damage locations are consistent with regions of high displacement gradient indicated by the moire fringe contour and also consistent with experimental observations. Delamination was observed around the cutout and may be responsible for the discrepancy between the analytical and experimental failure loads with the panel exhibiting a catastrophic failure at a larger end-shortening value than experimentally observed value.

3.4.3. Curved panel with a cutout of size $d/W=0.6$. The results for the curved panel with a cutout ratio (d/W) of 0.6 is presented in Figure 14, where the load is plotted versus the end-shortening displacement. The open symbols representing *FV1*, *FV2* and *FV3* indicate the load level at which damage described by field variable *FV1* through *FV3* initiated. Damage initiated before buckling of the panel occurred. The analyses and experimental results are in good agreement for most part of the curve. The final failure load obtained from the experiment is 25.2 kips. The final failure load obtained from progressive failure analysis is about 22.3 kips for the perfect panel and 22.5 kips for the imperfect panel which is about 10% less than the experimental failure load. However, both imperfect panel and perfect panel failed at approximately

the same end-shortening which is close to the experimental end-shortening at failure. Damage initiation starts as fiber-matrix shear (*FV2*) and fiber (*FV3*) failure at a load level of 16.6 kips for the geometrically perfect and imperfect panel. A postbuckling analysis for the geometrically imperfect panel predicts no load drop for this panel.

All the failure modes initiate near the edge of the cutout. Figure 15 shows a fringe plots of damage in the bottom ply after the final failure load for the geometrically imperfect panel. These damage locations are consistent with regions of high displacement gradient indicated by the moire fringe pattern and compare well with experimental observations. Delamination was observed around the cutout region.

3.5. Bead-stiffened Panel Loaded in Shear. The thermoformed bead-stiffened configuration is an advanced concept for stiffened graphite thermoplastic panels. Thermoforming is a cost effective manufacturing method for incorporating bead stiffeners. An experimental and analytical investigation of these bead-stiffened panels was conducted by Rouse [27]. The bead-stiffened panels were loaded in in-plane shear loading using a picture frame fixture similar to the one described above. It was found that the bead stiffened panels failed near the curved tip of the stiffener where large magnitudes of stress resultants were predicted.

The bead-stiffened panel has a laminate stacking sequence of $[\pm 45 / \pm 45 / 0 / \pm 45 / 90]_s$ with a nominal ply thickness of 0.005-in. The mechanical properties of the material are $E_{11}=18.0$ Msi, $E_{22}=1.50$ Msi, $G_{12}=G_{13}=G_{23}=0.82$ Msi. The allowables are $X_t=300.0$ ksi, $X_c=210.0$ ksi, $Y_t=13.0$ ksi, $Y_c=31.0$ ksi, $S_{c12}=S_{c13}=27.0$ Ksi, and $S_{c23}=5.0$ ksi. A finite element model of the bead-stiffened panel is shown in Figure 16. This model consists of 2935 nodes and 2849 elements. No geometric imperfection was added to the model of the bead-stiffened panel. Three integration points through each ply thickness are used in the analysis for the computation of section properties.

The results for this in-plane shear-loaded panel are shown in Figure 17, where the load is plotted versus the axial strain (ϵ_{xx}) in the top and bottom plies (45° ply) at the center of the test panel. The curves *FV1*, *FV2*, and *FV3* indicate the load level at which damage modes described by the field variable *FV1* through *FV3* initiate. The analytical results are in good agreement with the experimental results. The final failure load obtained from the experiment is 27.9 kips, which is 12 % less than the final failure load of 24.4 kips obtained from the progressive failure analysis of 24.4 kips. Damage initiation starts as matrix cracking (*FV1*) at a load level of 10.8 kips, whereas both fiber-matrix shear (*FV2*) and fiber failure are initiated at the same load level of 12.8 kips. Hence the structure can carry an additional load of approximately 17.0 kips (60% of the final experimental load) after the initiation of matrix cracking damage. Even after initiation of fiber-matrix shear and fiber failure, the panel can carry an additional load of approximately 15.0 kips (53% of the final experimental load).

A contour plot of the out-of-plane deflection is shown in Figure 18(a) and fringe plots for matrix cracking, fiber-matrix shear, and fiber failure in the top ply after the final failure load are shown in Figure 18(b) through 18(d). The damage initiated near the curved tip of the bead-stiffener and propagated to the other regions as shown in these figures. The locations for damage occurred within the region of high displacement gradient as shown in Figure 18(a) and are consistent with experimental observations. For the case of this stiffened panel, initial geometric imperfections are not a critical factor in predicting the observed behavior.

4. Concluding Remarks. The results of an analytical and experimental study to evaluate the initiation and progression of damage in nonlinearly deformed stiffened and unstiffened panel are presented. These studies are also conducted for panels with cutouts and subjected to two loading conditions. The progressive

failure methodology includes matrix cracking, fiber-matrix shear, and fiber failure, but ignores delamination failure. The effect of initial geometric imperfections is also investigated as part of the study.

For a flat panel loaded in in-plane shear loading, the three failure modes considered in the study accurately represent the damage scenario in the postbuckling regime. The analytically determined response, failure modes and damage locations compare well with the experimental results when the initial geometric imperfection is included in the analysis in a simple manner. When a cutout is introduced, however, delamination occurs at the hole boundary as an additional failure mode resulting in some discrepancies with the analytical behavior. The analysis results for a flat plate with a cutout predict a final failure load being approximately 10% greater than the experimental failure load.

The response of curved panels with and without cutouts are studied with the panel loaded in compression. When measured geometric imperfection is included in both curved panel models, the response of the panel without cutout compares well with experimental results. No delamination occurs for this case and the failure modes considered in this paper develop after panel buckling. For the curved panel with a cutout, however delamination does occur at the free edge of the hole with the panel failing catastrophically. Unlike the panel without a cutout, the panel with a cutout exhibits no residual strength. It may be important to include delamination failure mode to predict the residual strength of curved panels with a cutout of the type considered here.

For the bead-stiffened panel response, failure modes and damage locations are well predicted by the analysis results. The residual strength values from the analysis and experiment are within 12 percent.

REFERENCES

- [1] R. TALREJA, *Modeling of Damage Development in Composites using Internal Variable Concepts*, Damage Mechanics in Composites, AD Volume 12, Proceedings of the ASME Winter Annual Meeting, Boston, MA, pp. 11-16, 1987.
- [2] D. H. ALLEN, C. HARRIS, AND S. E. GROVES, *A Thermomechanical Constitutive Theory for Elastic Composites with Distributed Damage, Part I. Theoretical Development*, International Journal of Solids and Structures, 23, No. 9 (1987), pp. 1301-1318.
- [3] F.-K. CHANG AND K. Y. CHANG, *A Progressive Damage Model for Laminated Composites Containing Stress Concentrations*, Journal of Composite Materials, 21 (Sept. 1987), pp. 834-855.
- [4] A. K. PANDEY AND J. N. REDDY, *A Post First-Ply Failure Analysis of Composite Laminates*, AIAA Paper 87-0898, Proceedings of the AIAA/ASME/ASCE/AHS/ASC 28th Structures, Structural Dynamics, and Material Conference, pp. 788-797, 1987.
- [5] O. O. OCHOA AND J. J. ENGBLOM, *Analysis of Failure in Composites*, Composite Science and Technology, 28 (1987), pp. 87-102.
- [6] F.-K. CHANG AND L. B. LESARD, *Damage Tolerance of Laminated Composites Containing an Open Hole and Subjected to Compressive Loadings: Part 1-Analysis*, Journal of Composite Materials, 25 (Jan. 1991), pp. 2-43.
- [7] L. MINNETYAN, C. C. CHAMIS, AND P. L. N. MURTHY, *Structural Behavior of Composite with Progressive Fracture*, Journal of Reinforced Plastics and Composite, 11 (April 1992), pp. 413-442.
- [8] S. P. ENGELSTAD, J. N. REDDY, AND N. F. KNIGHT, *Postbuckling Response and Failure Prediction of Graphite-Epoxy Plates Loaded in Compression*, AIAA Journal, 30, No. 8 (August 1992), pp. 2106-2113.

- [9] I. SHAHID AND F. K. CHANG, *An Accumulative Damage Model for Tensile and Shear Failures of Laminated Composite Plates*, Journal of Composite Materials, 29, No. 7 (1995), pp. 926-981.
- [10] T. W. COATS AND C. E. HARRIS, *Experimental Verification of a Progressive Damage Model for IM7/5260 Laminates subjected to Tension Fatigue*, Journal of Composite Materials, 29, No. 3 (1995), pp. 280-305.
- [11] D. W. SLEIGHT, N. F. KNIGHT, JR., AND J. T. WANG, *Evaluation of a Progressive Failure Analysis Methodology for Laminated Composite Structures*, Proceedings of the 38th AIAA/ASME/ASCE/AHS/ASC Structures, Structural Dynamics, and Materials Conference, Reston, VA, pp. 2257-2272, 1997.
- [12] E. MOAS AND O. H. GRIFFIN, JR., *Progressive Failure Analysis of Laminated Composite Structure*, AIAA Paper 97-1186, Proceedings of the AIAA/ASME/ASCE/AHS/ASC 38th Structures, Structural Dynamics, and Material Conference, pp. 2246-2256, 1997.
- [13] S. B. SINGH, ASHWINI KUMAR, AND N. G. R. IYENGAR, *Progressive Failure of Symmetrically Laminated Plates under uniaxial Compression*, Structural Engineering and Mechanics, 5 (1997), pp. 433-450.
- [14] S. B. SINGH AND A. KUMAR, *Postbuckling Response and Failure of Symmetric Laminates under In-Plane Shear*, Composite Science and Technology, 58 (1998), pp. 1949-1960.
- [15] L. N. B. GUMMADI AND A. N. PALAZOTTO, *Progressive Failure Analysis of Composite Shells considering Large Rotations*, Composite Part B, 29 (1998), pp. 547-563.
- [16] D. HUANG AND L. MINNETYAN, *Computational Simulation of Progressive Fracture in J-Stiffened Composite Shear Panels in Postbuckling Range*, AIAA Paper 99-1356, Proceedings of the AIAA/ASME/ASCE/AHS/ASC 40th Structures, Structural Dynamics, and Material Conference, pp. 1353-1362, 1999.
- [17] C. G. DÁVILA, D. R. AMBUR, AND D. M. MCGOWAN, *Analytical Prediction of Damage Growth in Notched Composite Panels Loaded in Compression*, Journal of Aircraft, 37, No. 5 (Sept.-Oct. 2000), pp. 898-905.
- [18] A. T. BARANSKI AND S. B. BIGGERS, *Postbuckling Analysis of Tailored Composite Plates with Progressive Failure*, Composite Structures, 46 (1999), pp. 245-255.
- [19] N. F. KNIGHT, C. C. RANKIN, F. A. AND BROGAN, *Controlling A Nonlinear Solution Procedure During a Progressive Failure Analysis*, AIAA Paper No. 2000-1460, April 2000.
- [20] R. C. AVERILL, *A Micromechanics-Based Progressive Failure Model for Laminated Composite Structures*, Proceedings of the 33rd AIAA/ASME/ASCE/AHS/ASC Structures, Structural Dynamics, and Materials Conference, AIAA, Washington, DC, pp. 2898-2904, 1992.
- [21] Z. HASHIN, *Failure Criteria for Unidirectional Fiber Composites*, Journal of Applied Mechanics, 47 (June 1980), pp. 329-334.
- [22] *ABAQUS User's Manual*, Vol. 3, Ver. 5.6, Hibbitt, Karlsson, and Sorensen, Pawtucket, RI, pp. 25.2.33-1, 1996.
- [23] *ABAQUS Example Problems Manual*, Vol. 1, Ver. 5.5, Hibbitt, Karlsson, and Sorensen, Pawtucket, RI, pp. 3.2.25.25-1, 1995.
- [24] M. ROUSE, *Post-Buckling of Flat Unstiffened Graphite-Epoxy Plates Loaded in Shear*, Presented at the AIAA/ASME/ASCE/AHS 26th Structures, Structural Dynamics, and Materials Conference, Orlando, FL, April 15-17, 1985. Also AIAA Paper No. 85-0771-CP.
- [25] M. W. HILBURGER, V. O. BRITT, AND M. P. NEMETH, *Buckling Behavior of Compression-loaded*

Quasi-isotropic Curved Panel with a Circular Cutout, 40th AIAA/ASME/ASCE/AHS/ASC Structures, Structural Dynamics and Materials Conference, St. Louis, MO, Paper AIAA-99-1279, April 12-15, 1999.

- [26] M. ROUSE, *Effect of Cutouts or Low-speed Impact Damage on the Postbuckling Behavior of Composite Plates Loaded in Shear*, Presented at the AIAA/ASME/ASCE/AHS 31th Structures, Structural Dynamics, and Materials Conference, Long Beach, CA, April 2-4, 1990. Also AIAA Paper No. 90-0966-CP.
- [27] M. ROUSE, *Structural Response of Bead-stiffened Thermoplastic Shear Webs*, First NASA Advanced Composite Technology Conference, Oct. 29-Nov. 1, 1990, NASA Conference Publication 3104, pp. 969-977.

Table 1: Summary of Evolution of Progressive failure.

Researchers	Analysis type	Structure type	Loading condition	Experimental Co-relation
1987				
Chang & Chang ([3])	LG	Plate with a cutout	Tension	yes
Pandey & Reddy ([4])	LG	Plate with a cutout	Tension	no
Ochoa & Engblom ([5])	LG	Plate, beam	Tension, bending	no
1991				
Chang & Lesard ([6])	LG	Plate with a cutout	Compression	yes
1992				
Minnetyan et al. ([7])	LG	Plate with a cutout	Tension	no
Engelstad et al. ([8])	NLG	Plate with & without a cutout	Compression (PB)	yes
1995				
Shahid & Chang ([9])	LG	Plate	Tension, shear	yes
Coats & Harris ([10])	LG	Plate with a cutout	Tension	yes
1997				
Sleight et al. ([11])	NLG	Unstiffened & stiffened panel with & without a cutout	Compression (PB)	yes
Moas & Griffin ([12])	NLG	Curved frame	Transverse	yes
Singh et al. ([13])	NLG	Plate	Compression (PB)	no
1998				
Singh & Kumar ([14])	NLG	Plate	Shear (PB)	no
Gummadi et al ([15])	NLG	Curved panel	Transverse	no
1999				
Huang et al. ([16])	NLG	J-stiffened panel	Shear (PB)	yes
Davila et al. ([17])	NLG	Stiffened panel with a cutout	Compression	yes
Baranski et al. ([18])	NLG	Plate	Compression (PB)	no
2000				
Knight et al. ([19])	NLG	Plate	Compression (PB)	yes
LG = Linear geometric, NLG = Nonlinear geometric, PB = Postbuckling				

Table 2: Dependence of material elastic properties on the field variables

No failure	Matrix cracking	Fiber-matrix shear	Fiber failure
E_{11}	E_{11}	E_{11}	$E_{11} \rightarrow 0$
E_{22}	$E_{22} \rightarrow 0$	E_{22}	$E_{22} \rightarrow 0$
ν_{12}	$\nu_{12} \rightarrow 0$	$\nu_{12} \rightarrow 0$	$\nu_{12} \rightarrow 0$
G_{12}	G_{12}	$G_{12} \rightarrow 0$	$G_{12} \rightarrow 0$
G_{13}	G_{13}	$G_{13} \rightarrow 0$	$G_{13} \rightarrow 0$
G_{23}	G_{23}	G_{23}	$G_{23} \rightarrow 0$
$FV1=0$	$FV1=1$	$FV1=0$	$FV1=0$
$FV2=0$	$FV2=0$	$FV2=1$	$FV2=0$
$FV3=0$	$FV3=0$	$FV3=0$	$FV3=1$

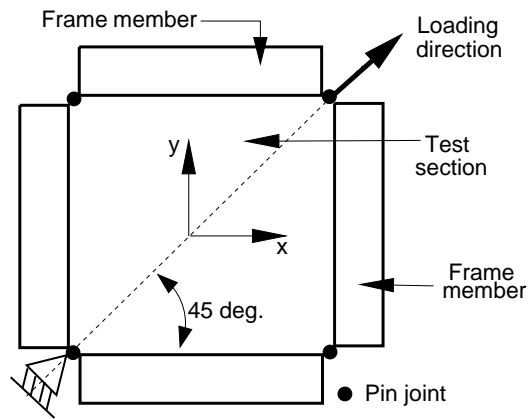


Figure 1: Schematic diagram of picture frame test fixture.

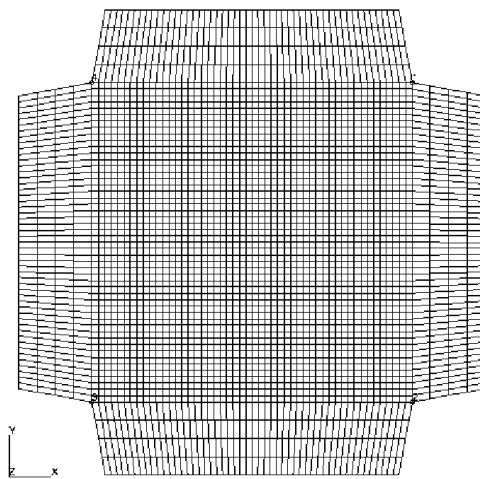


Figure 2: Finite element model of a flat composite panel in the picture frame test fixture.

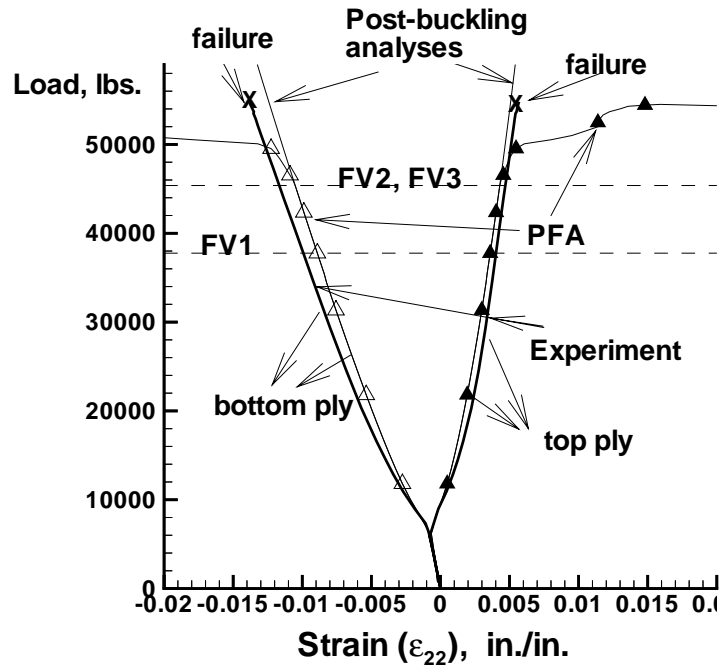


Figure 3: Load vs. strain component normal to fiber direction results in top and bottom plies of flat panel loaded in shear.

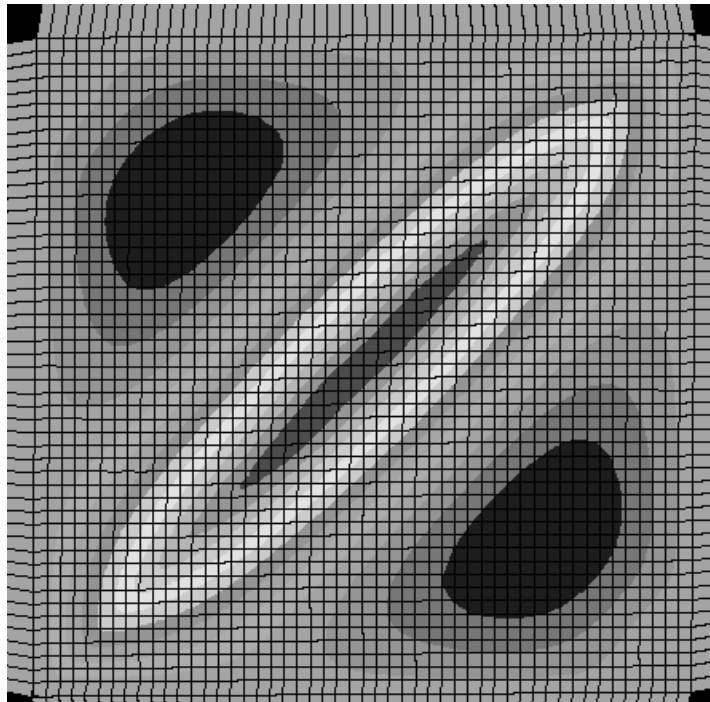
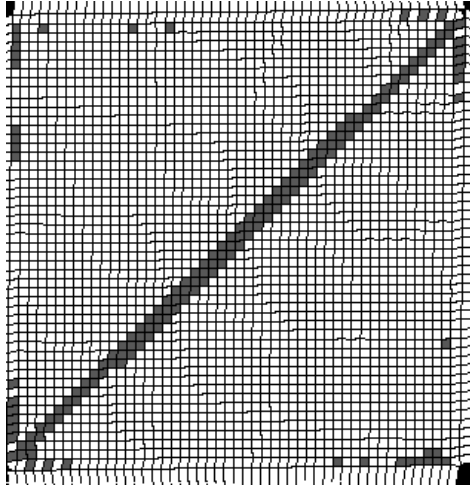
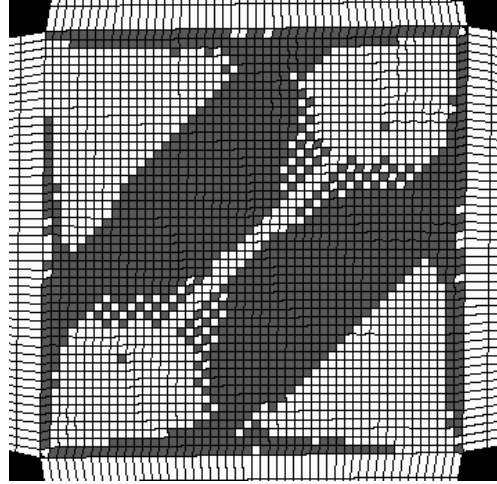


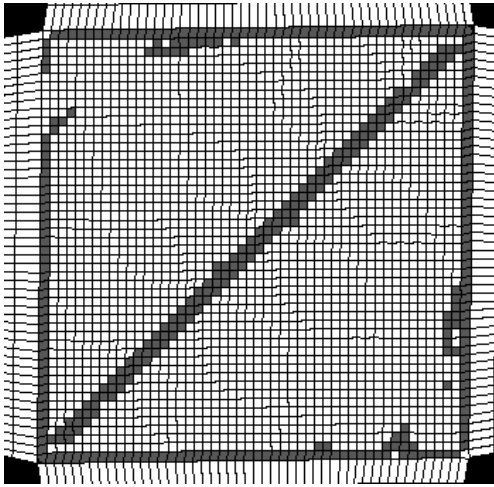
Figure 4: Out-of-plane deflection contour for flat panel in the post-buckling regime.



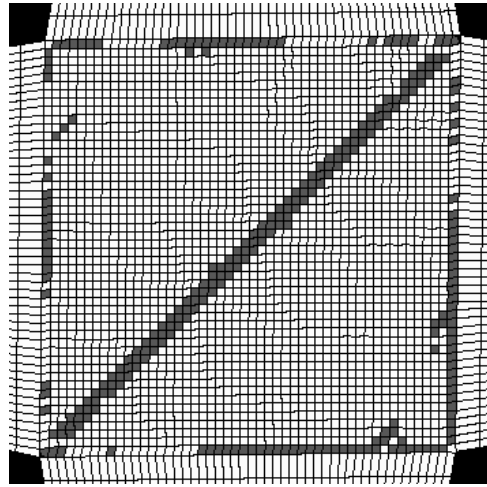
(a) Fringe plot of matrix cracking (FV1) in the top 45° ply



(b) Fringe plot of matrix cracking (FV1) in the bottom -45° ply



(c) Fringe plot of fiber-matrix shear (FV2) in the bottom -45° ply



(d) Fringe plot of fiber failure (FV3) in the bottom -45° ply

Figure 5: Fringe plot of damage in flat panel subjected to shear loading after final failure.

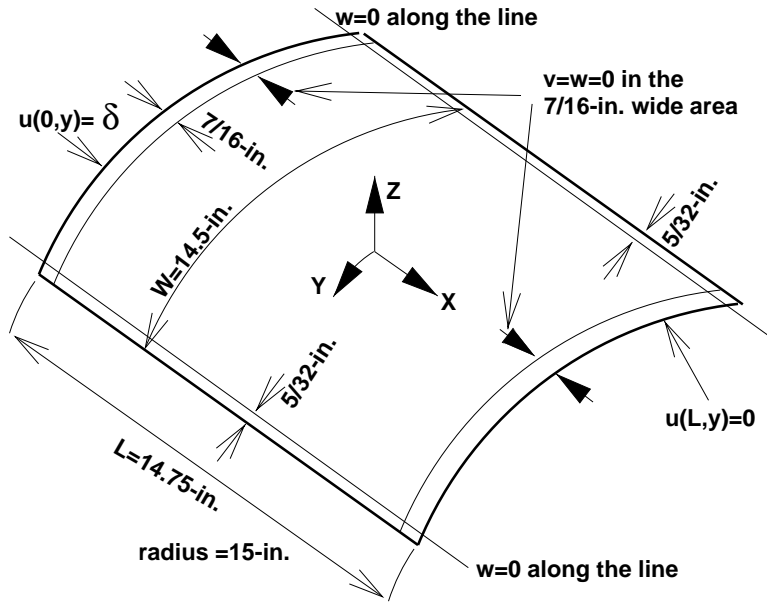


Figure 6: Geometry and boundary conditions for the curved composite panel.

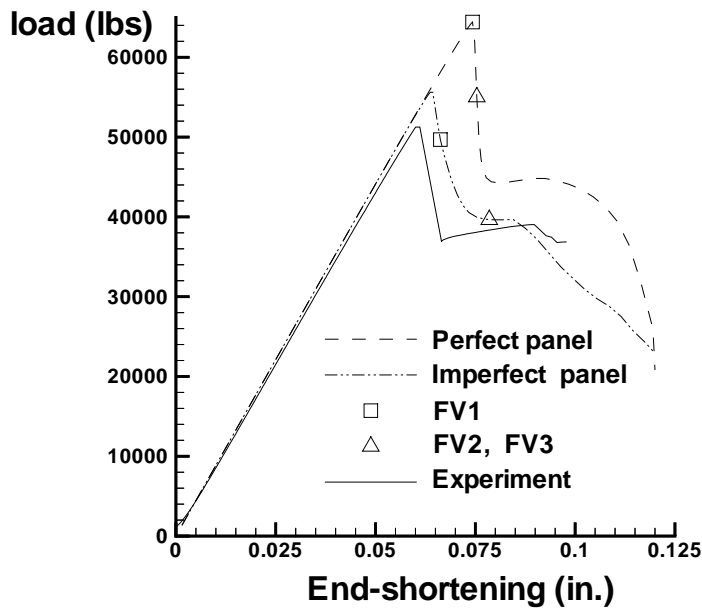
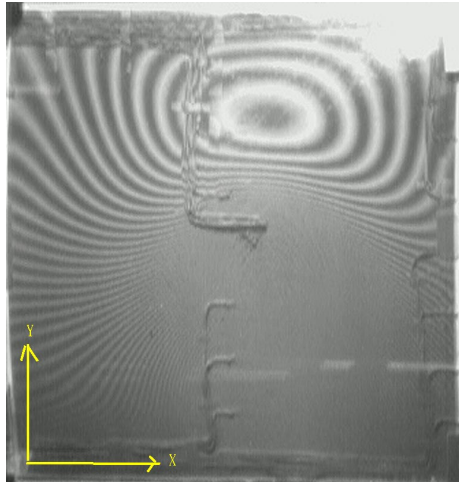


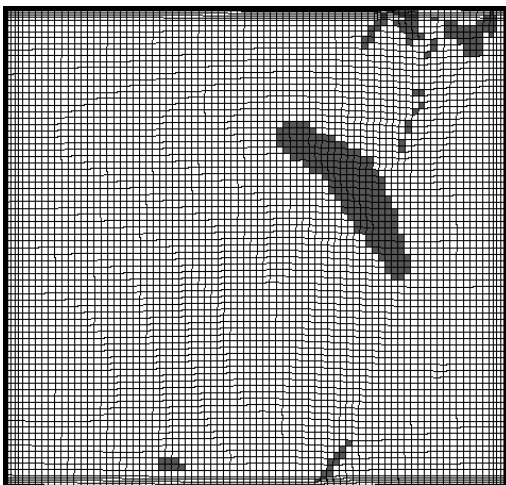
Figure 7: Load vs. end-shortening displacement results for the curved panel loaded in axial compression.



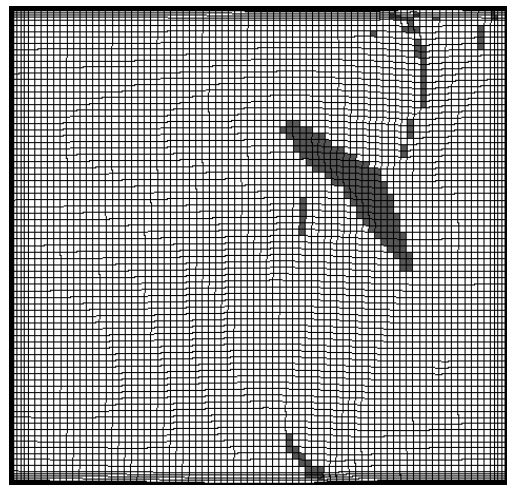
(a) Experimental out-of-plane displacement contour at failure



(b) Fringe plot of matrix cracking (FV1) in the bottom 45° ply



(c) Fringe plot of fiber-matrix shear failure (FV2) in the bottom 45° ply.



(d) Fringe plot of fiber failure (FV3) in the bottom 45° ply

Figure 8: Axial compression response and damage modes in curved panel after final failure.

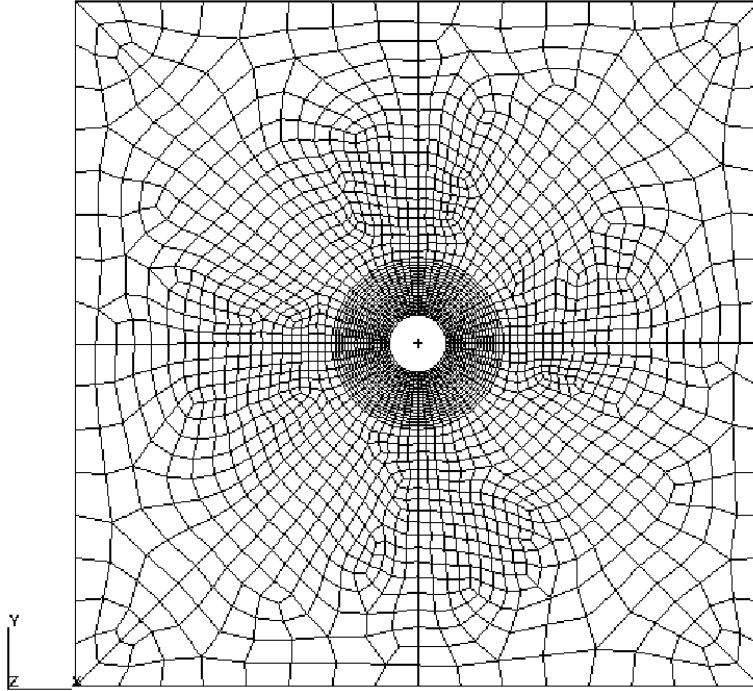


Figure 9: Finite element model of flat panel with a circular cutout.

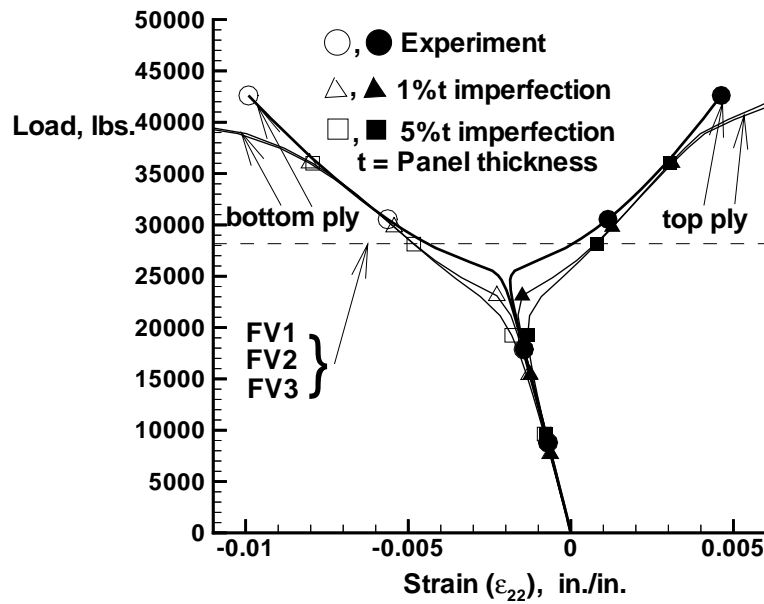


Figure 10: Load vs. strain component normal to fiber direction in the top and bottom plies of flat panel with a cutout loaded in shear.

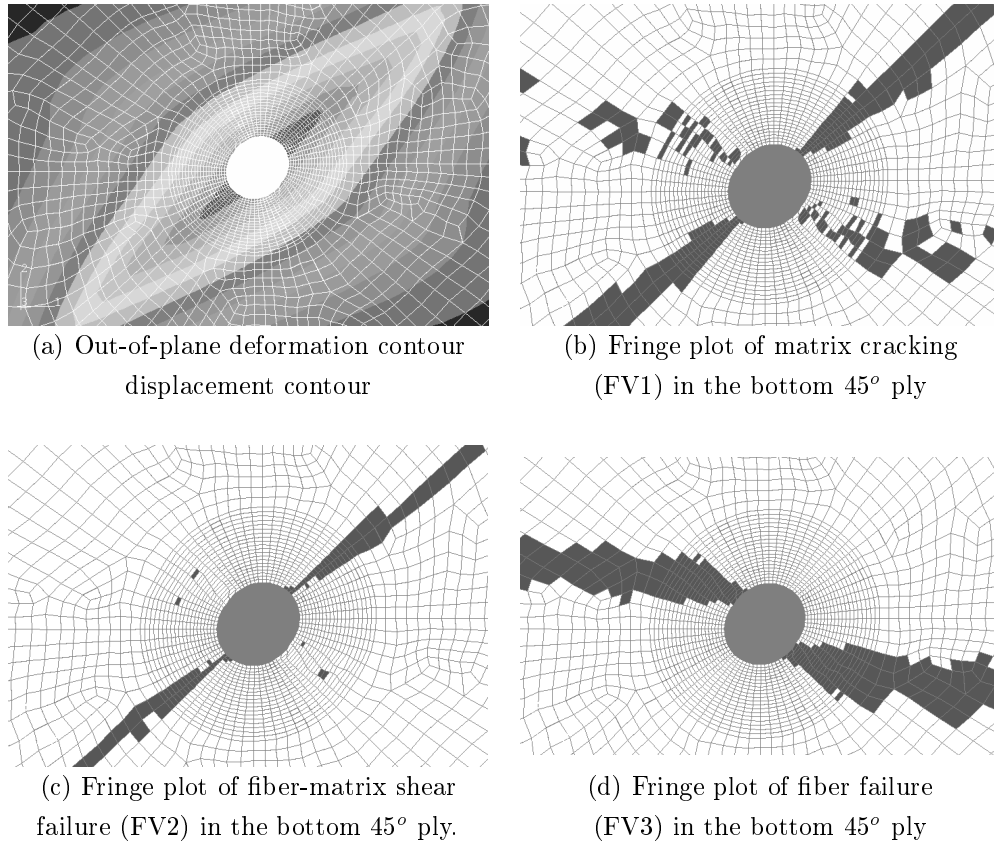


Figure 11: Analytical response and damage mode for a flat panel with a cutout and loaded in shear after final failure.

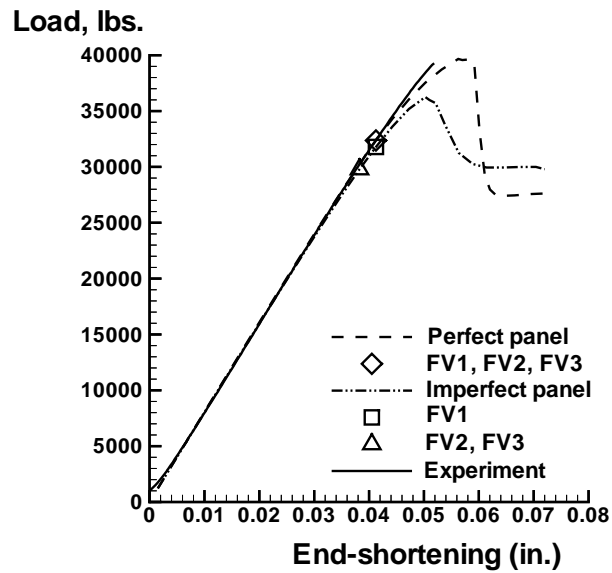


Figure 12: Load versus end-shortening displacement results for a curved panel with cutout ($d/W=0.2$) and subjected to axial compression loading.

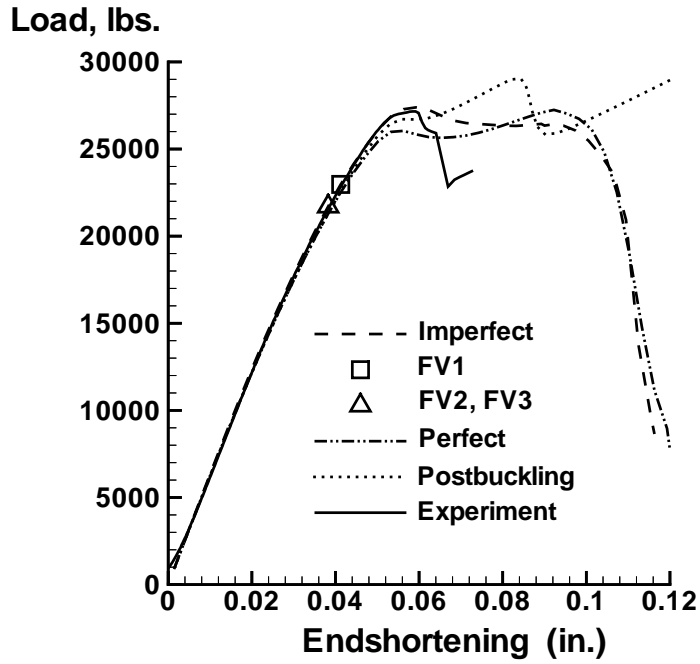


Figure 13: Load versus end-shortening displacement results for a curved panel with cutout ($d/W=0.4$) and subjected to axial compression loading.

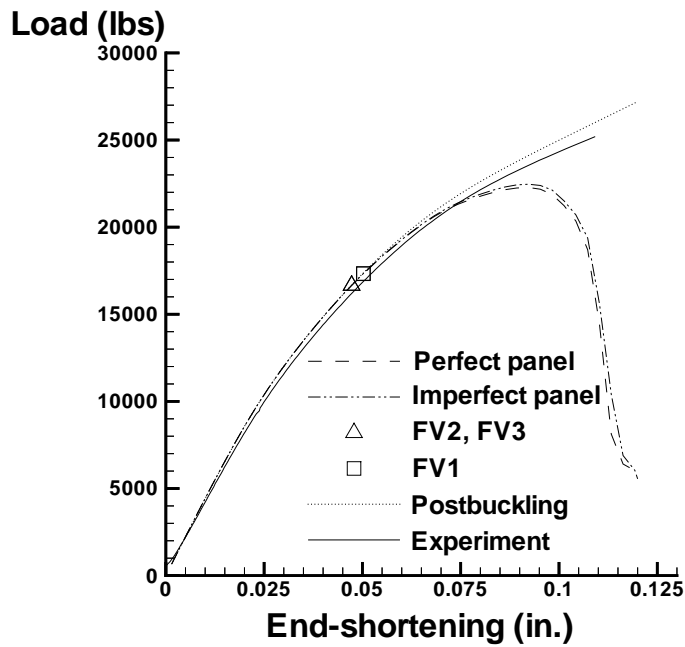
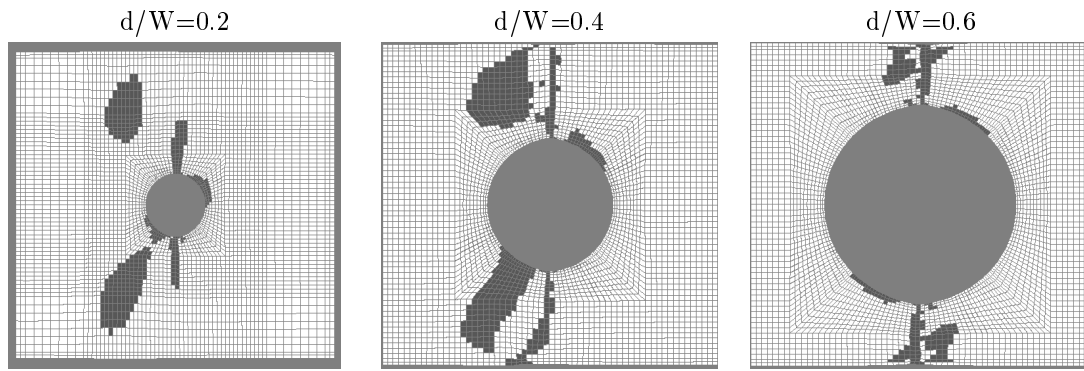
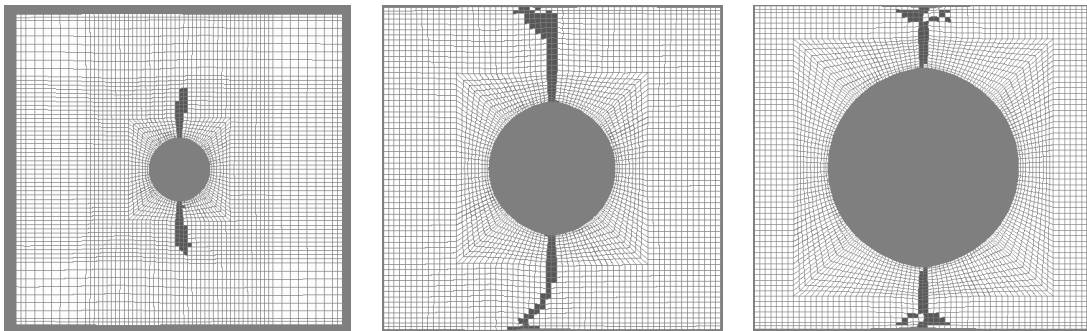


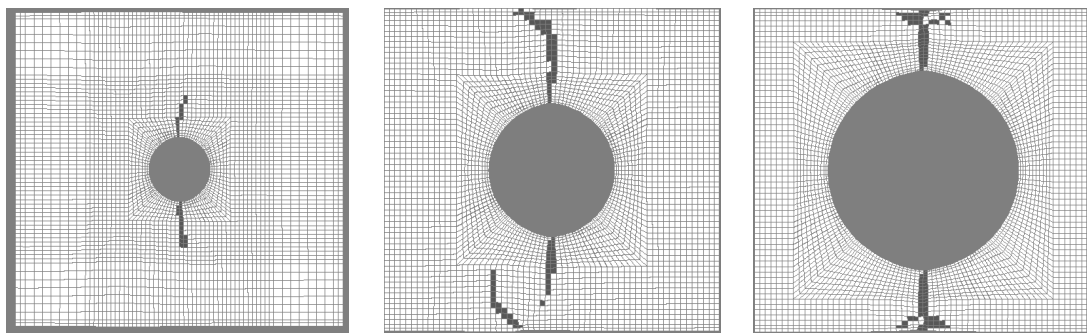
Figure 14: Load versus end-shortening displacement results for a curved panel with cutout ($d/W=0.6$) and subjected to axial compression loading.



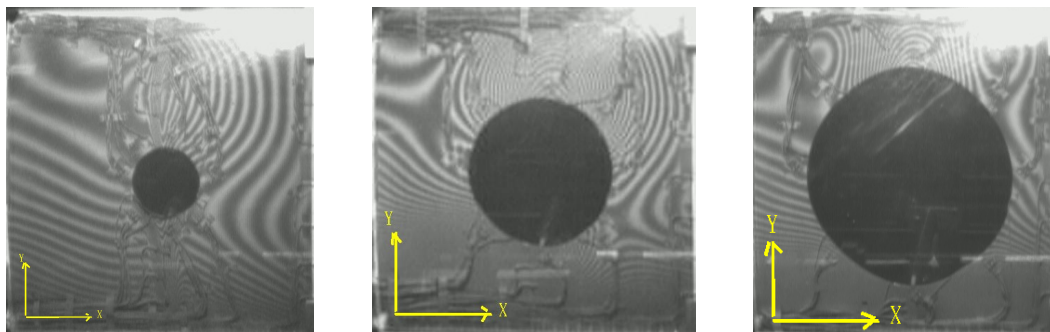
a. Fringe plot of matrix cracking in bottom ply (45°)



b. Fringe plot of fiber-matrix shear in bottom ply (45°)



c. Fringe plot of fiber failure shear in bottom ply (45°)



d. Out-of-plane displacement contour

Figure 15: Damage fringe plots and out-of-plane displacement contours for curved panels with cutouts and loaded in compression after final failure.

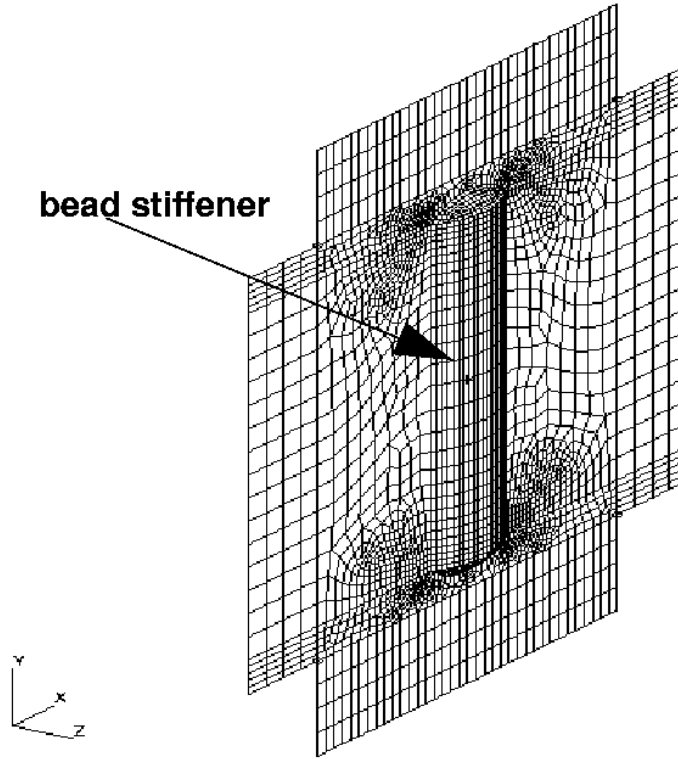


Figure 16: Finite element model of the bead-stiffened panel in picture frame test fixture.

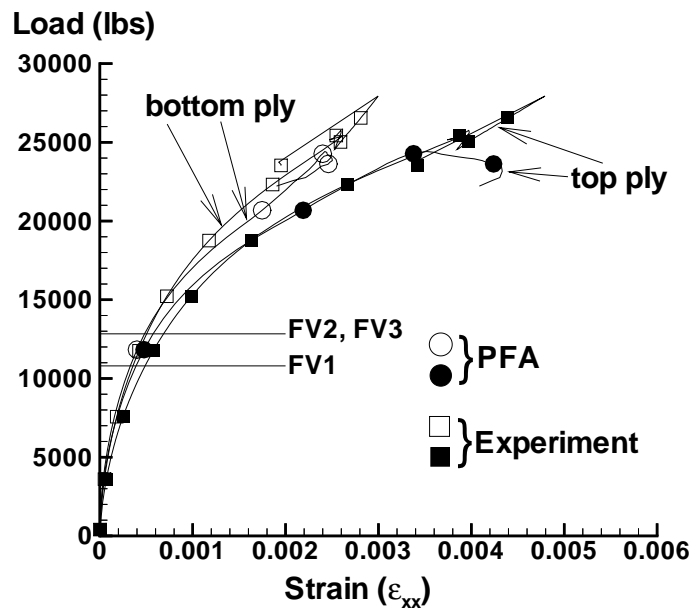
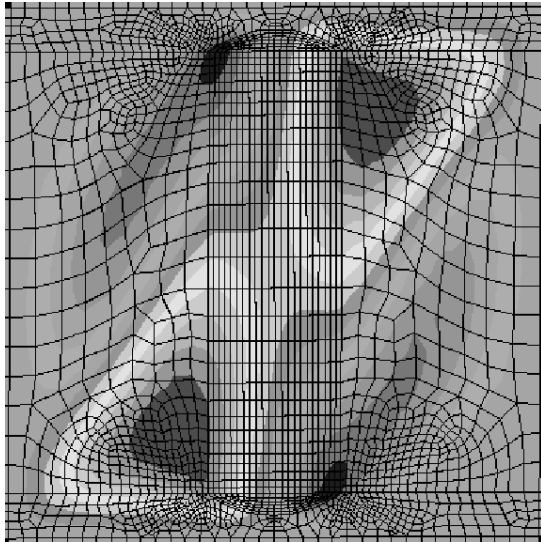
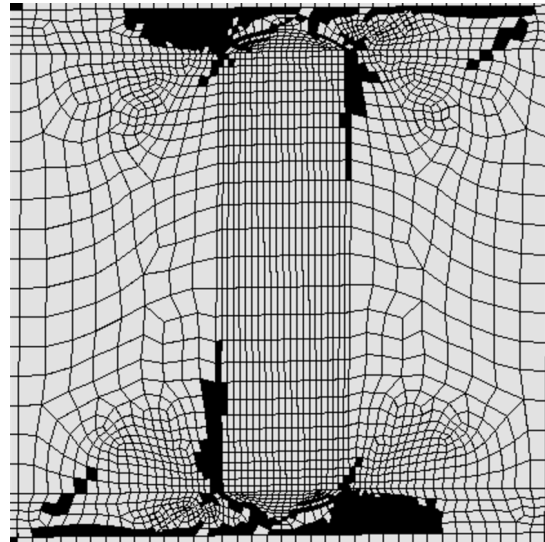


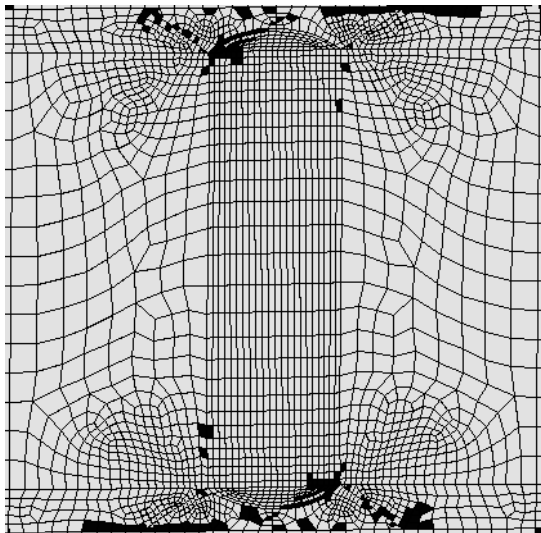
Figure 17: Load versus axial strain, (ϵ_{xx}) results at the center of bead-stiffened panel.



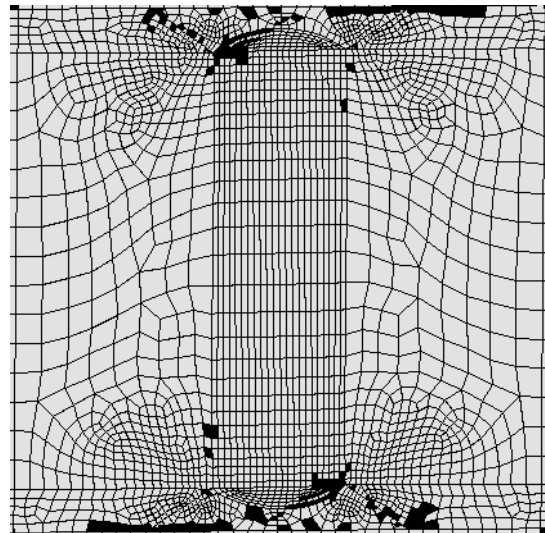
(a) Out-of-plane deformation contour displacement contour after failure



(b) Fringe plot of matrix cracking (FV1) in the top 45° ply



(c) Fringe plot of fiber-matrix shear failure (FV2) in the top 45° ply.



(d) Fringe plot of fiber failure (FV3) in the top 45° ply

Figure 18: Fringe plot of damage for the bead-stiffened panel after failure.